Research Article | Vol. 30, No. 7 / 28 Mar 2022 / Optics Express 10758
Optics EXPRESS

Detecting cylindrical vector beams with an on-chip plasmonic spin-Hall metalens

YANAN FU,[1] YULONG WANG,[1] YUQUAN ZHANG,[1] YEJUN HE,[2] CHANGJUN MIN,[1,3] AND XIAOCONG YUAN[1,4]

[1]*Nanophotonics Research Center, Shenzhen Key Laboratory of Micro-Scale Optical Information Technology & Institute of Microscale Optoelectronics, Shenzhen University, Shenzhen, China*
[2]*The College of Electronics and Information Engineering, Shenzhen University, Shenzhen 518060, China*
[3]*cjmin@szu.edu.cn*
[4]*xcyuan@szu.edu.cn*

Abstract: In recent years, singular optical beams, including optical vortex (OV) beams with phase singularities and cylindrical vector beams (CVBs) with polarization singularities, have brought new degrees of freedom for many applications. Although there have been various microscale devices for OV detection, the detection of CVBs with a microscale device is still a challenge. Here, we propose a new method for detection of CVBs with a designed on-chip plasmonic spin-Hall metalens structure. The focal position of the metalens and the splitting effect of at focus are studied in both an analytical model and numerical simulation. The results demonstrate that the metalens can not only detect different polarization orders of incident CVBs but also have an ability to distinguish radial, azimuthal and other vectorial polarization states under the same order of CVBs. This method has potential applications in compact integrated optical communication and processing systems.

1. Introduction

As a branch of modern optics, singular optics has attracted broad research interests over the past decades [1]. Phase singularity and polarization singularity are two typical optical singularities, and their representative light beams are optical vortex (OV) beams [2] and cylindrical vector beams (CVBs) [3], respectively. Due to the degree of freedom of orbital angular momentum (OAM), OV beams have widely been studied and applied in various optical fields, including imaging and metrology [4,5], optical tweezers [6,7], optical sensing [8,9], quantum optics [10], and optical communication [11,12]. Like OV beams, the CVBs have the degree of freedom of vectorial polarization order, that is, different polarization orders of CVBs are orthogonal to each other [13]. Moreover, for each order of CVB, there are two orthogonally radial and azimuthal modes, which further enhances the capacity of CVBs as multiplexed channels in optical communication [14]. In addition, CVBs has also been widely used in other fields such as super-resolution imaging [15], optical tweezers [16], and longitudinal optical needles [17], owing to its unique tight focusing and polarization characteristics [18].

Motivated by the great potential of CVBs, various methods have been developed for generating CVBs, including active and passive ways [19–21]. The detection of singularity beams is very important for their applications. In particular, the development of on-chip detection methods and devices plays an important role in the application of integrated optics and nanophotonics. In recent years, a variety of on-chip OAM detection methods and microscale devices have been reported, such as plasmonic OAM detector [22–24]. By contrast, the researches of on-chip CVB detection methods and microscale devices are much less. Traditional methods for detecting CVBs are usually based on optical diffraction and interference devices, such as q-plate [25,26], diffraction grating [27,28] and geometric transformation [29], and thus have shortcomings of the requirement of multiple devices and large volume of optical system, strongly limiting their

#455148 https://doi.org/10.1364/OE.455148
Journal © 2022 Received 31 Jan 2022; revised 27 Feb 2022; accepted 28 Feb 2022; published 15 Mar 2022

Optics EXPRESS

application in compact and integrated optical systems. Thus, how to realize the detection of CVB with on-chip microscale devices is still a challenge.

In recent years, metasurface devices have deeply been investigated and showed powerful capability of manipulating light field in micro- and nano-scale [30–33]. Many previous reports demonstrate that ultracompact on-chip metasurface can achieve nearly arbitrary control of optical phase and polarization, including anomalous (directional and focusing/diverging) launching [34–35] and wavefront engineering of evanescent waves and surface plasmon polaritons (SPPs) [36,37], generation and directional coupling of plasmonic vortices [38,39], mode-selective coupling with polarization sensitivity [40] and on-chip polarization multiplexing [41], verifying that it can be a promising candidate for on-chip CVB detection.

In this work, we propose a new method for CVB detection based on an on-chip plasmonic spin-Hall metalens structure. The designed metalens is composed of spin-sensitive unit cells in a gold nano-film, and enables the generation of single SPP focus under the incidence of CVB. The position of the SPP focal point shifts with different orders of CVBs, hence the order of CVB can be detected by the focal position. Besides the different orders of CVBs, both analytical and simulated results show that the designed metalens can also distinguish the orthogonally radial and azimuthal modes under the same CVB order, even other vectorial polarization state between the radial and azimuthal modes can be judged according to the splitting effect of the SPP focus, which is superior than many previous designs [42–45]. The proposed structure has great potential in compact integrated CVB-multiplexing communication and processing systems.

2. Principle of the metalens

The schematic illustration of the proposed on-chip plasmonic spin-Hall metalens is shown in Fig. 1(a). The metalens consists of two semicircular parts with orthogonally oriented nano-slit pairs on a gold film (200 nm thickness) and glass substrate. The upper half semicircular part of the structure (indicated by red dashed box) and the lower half part (indicated by grey dashed box) are used to focus SPPs excited by the right-handed and left-handed circularly polarization components of the incident CVB, respectively. The wavelength of incident CVB is 632.8 nm, which is normally incident to the structure from the bottom. When a CVB of a certain order is incident, the nano-slits of the metalens excite SPP and then form a strong SPP focus in the center region as shown in Fig. 1(a), and the focal spot shifts with the change of CVB order.

Taking one of the semicircular parts as example, the schematic diagram with parameters is shown in Fig. 1(b) to introduce the spin-Hall effect of SPP propagation. The radial vector is $\hat{e}_c$, and the azimuthal vector is $\hat{e}_t$. θ is the angle between the radius and the y-axis. The distance between the two nano-slits of a pair is $s = \lambda_{spp}/4$ (λ_{SPP} is the SPP wavelength) in both the radial and azimuthal directions. The width and length of all nano-slits are 60 nm and 240 nm, respectively. The period of the nano-slit pairs in the azimuthal direction is $P_t = \lambda_{SPP}$. According to previous report [35], such orthogonal nano-slits can achieve spin-polarization-controlled directional coupling of SPPs. For left-handed circularly polarized (LCP) and right-handed circularly polarized (RCP) light, the SPP excited by the semicircular structure in Fig. 1(b) propagates inward and outward, resulting in focusing and divergence of SPP, respectively, which presents the spin-Hall effect of SPP. Therefore, the structure shown in Fig. 1(b) can be used as an on-chip spin-Hall metalens under LCP incidence. The other half of the whole metalens structure is symmetric with Fig. 1(b) about the x-axis, and the corresponding propagation behavior of SPP excited by LCP and RCP light is opposite to that in Fig. 1(b).

The incident CVB with order m can be described by the following Jones vector J_m:

$$J_m = \begin{pmatrix} \cos(m\varphi + \emptyset_0) \\ \sin(m\varphi + \emptyset_0) \end{pmatrix} = = \frac{1}{2} e^{i(m\varphi+\emptyset_0)} \begin{pmatrix} 1 \\ -i \end{pmatrix} + \frac{1}{2} e^{-i(m\varphi+\emptyset_0)} \begin{pmatrix} 1 \\ i \end{pmatrix} \tag{1}$$

Optics EXPRESS

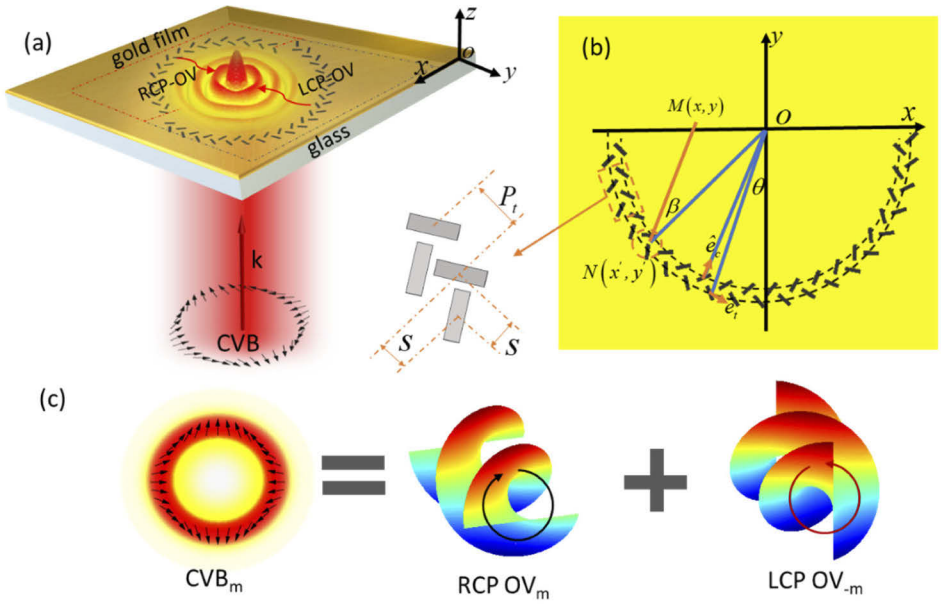

Fig. 1. (a) The schematic diagram of the on-chip plasmonic spin-Hall metalens structure. (b) The schematic diagram of the lower semicircular part of the metalens and the definition of structural parameters. The lower left corner is magnified view of the nano-slits. (c) The mth-order CVB is comprised of a LCP OV beam with a topological charge of $-m$ and a RCP OV beam with a topological charge of $+m$.

where m is the order of CVB, φ is the azimuthal angle, and $\emptyset_0$ is the initial phase angle [29]. It can be seen from Eq. (1) that an m-order CVB can be divided into a pair of conjugate OV beams, including an RCP OV with a topological charge of m and an LCP OV with a topological charge of $-m$ (as shown in Fig. 1(c)). The total angular momentum of these two parts is $j = \sigma + m$, where $\sigma$is the spin angular momentum with the value of σ =1 and -1 for LCP/RCP light, respectively. When an m-order CVB is incident on the structure as shown in Fig. 1(a), it is equivalent to an m-order RCP OV and an $-m$-order LCP OV to generate the focusing and divergence of SPP, respectively.

According to the 2-D Helmholtz and Kirchhoff integral theorem, the field distribution at any point $M(x, y)$ in the convergent SPP field generated by the metalens in Fig. 1(b) can be expressed as [46],

$$E_z(x,y,\omega) = \frac{ik_{spp}(\omega)R}{4}\{H_0^{(2)}(k_{spp}(\omega)R)H_1^{(1)}(k_{spp}(\omega)d)\cos\beta$$
$$-H_1^{(2)}\left(k_{spp}\left(\omega\right)R\right)H_0^{(1)}\left(k_{spp}\left(\omega\right)d\right)\Big\}\,U\left(\theta\right)exp\left(-ij\varphi\right)d\theta \tag{2}$$

where $k_{spp}(\omega) = 2\pi/\lambda_{spp}(\omega)$ is the wave vector of the SPP, ω is the angular frequency of the light source, R is the radius of the semi-ring structure, θ is the angle between the normal line NO at N on the semi-ring and the y-axis (Fig. 1(b)), and β is the angle between NO and MN. $d = \sqrt{(x'-x)^2+(y'-y)^2}$ is the distance between $M(x, y)$ and $N(x', y')$, $H_n^{(1)}(x)$ is the Hankel function of the first kind of order n, $H_n^{(2)}(x)$ is the Hankel function of the second kind of order n, $U(\theta)$ is the amplitude at any point $N(x', y')$ on the arc, $j = \sigma + m$ is the total angular momentum of LCP part of the incident CVB, φ represents the azimuth angle with $\tan\varphi = \frac{y}{x}$.

Optics EXPRESS

When $R \gg \lambda_{spp}$, the asymptotic expression of Hankel function in Eq. (2) is expressed as:

$$H_n^{(1)}(x) \approx \sqrt{\frac{2}{\pi x}} exp\left[i\left(x - \frac{n\pi}{2} - \frac{\pi}{4}\right)\right],$$

where n represents any integer. Then the E_z field of SPP at any point in the focal area of the metalens structure can be obtained as:

$$E_z(x, y, \omega) \approx \frac{\sqrt{R} exp[-ik_{spp}(\omega)R]}{2\pi} \int_{\Sigma} \frac{exp[ik_{spp}(\omega)d]}{\sqrt{d}} (1 + \cos\beta) U(\theta) exp(-ij\varphi) d\theta \quad (4)$$

According to Eq. (4), the distribution of SPP field excited by incident CVB with different order m can be calculated.

To verify the correctness of the above analytical model with Eqs. (1)-(4), its calculation results are compared with the numerical simulation results. All the simulations were carried out using the finite difference time domain method (Lumerical FDTD Solutions). The FDTD model built for the simulation of the on-chip metalens has a three-dimensional simulation range of 17 μm in both x and y direction and 2 μm in z direction. All boundaries for the simulation volume are terminated with perfectly matched layers (PML) to avoid parasitic unphysical reflections. The grid size is chosen as 20 nm in both x and y direction, and minimum 1 nm in z direction. The incident circularly-polarized light is composed of two orthogonal lineally-polarized plane-wave beams of equal intensity but with $\pm\pi/2$ phase difference. The CVB source script is written according to Eq. (1). The material of metal film is Au with relative permittivity from material database Au(gold)-CRC. The glass substrate is taken as a lossless material with a constant refractive index of 1.45.

3. Results and discussion

3.1. Structure design

Figure 2 shows the design flow of our metalens structure, as well as the theoretical calculation results and FDTD simulation results at each step. First, a common plasmonic lens [47,48] composed of a single semicircular slit with a radius of 3.6 μm ($\approx 6\lambda_{SPP}$) and a width of 0.3 μm are considered, as shown in the first line of Fig. 2. Three different incident lights are used to study its SPP focusing capability, including an LCP OV beam with topological charge $l = -3$ (Fig. 2(b)), an RCP OV beam with topological charge $l = 3$ (Fig. 2(c)), and a CVB with $m = 3$ and $\emptyset_0 = 0$ (Figs. 2(d)–2(e)). It can be observed that the semicircular slit can generate a single SPP focus for both the LCP/RCP OV beams, but cannot for the CVB. According to Eq. (1), CVB is actually the superposition of the LCP/RCP OV beams, so the field in Fig. 2(d) is actually the result of the coherent superposition of the fields in Fig. 2(c) and Fig. 2(b). As the SPP focus fields in Fig. 2(b) and Fig. 2(c) coherently interfere, multiple SPP hotspots are generated instead of a single focus.

Then, the single semicircular slit is replaced by a semicircular spin-Hall metalens (Fig. 2(f)) composed of nano-slit pairs (lower semi-part of the proposed metalens in Fig. 1(a)), and its SPP focusing properties under the same three incident lights are shown in Figs. 2(g)–2(j). It can be found that in this structure the LCP OV beam can generate single SPP focus, while the SPP generated by the RCP OV beam diverges towards the lower side, which is consistent with the theoretical predictions of the spin-Hall effect. The CVB can also generate single SPP focus (Fig. 2(i)) due to its LCP OV component. In Figs. 2(k)–2(o), the performance of the upper semi-part of the spin-Hall metalens is studied, whose radius of upper semi-ring is 3μm ($\approx 5\lambda_{SPP}$). It is obvious that the upper semi-part shows the opposite results to that of the lower semi-part, where the RCP OV and CVB can form single SPP focus but the LCP OV cannot, also owing to the spin-Hall effect. Finally, the whole metalens structure composed of both upper and lower semi-parts is studied in Figs. 2(q)–2(t). It can be found that all the three incident lights can

Optics EXPRESS

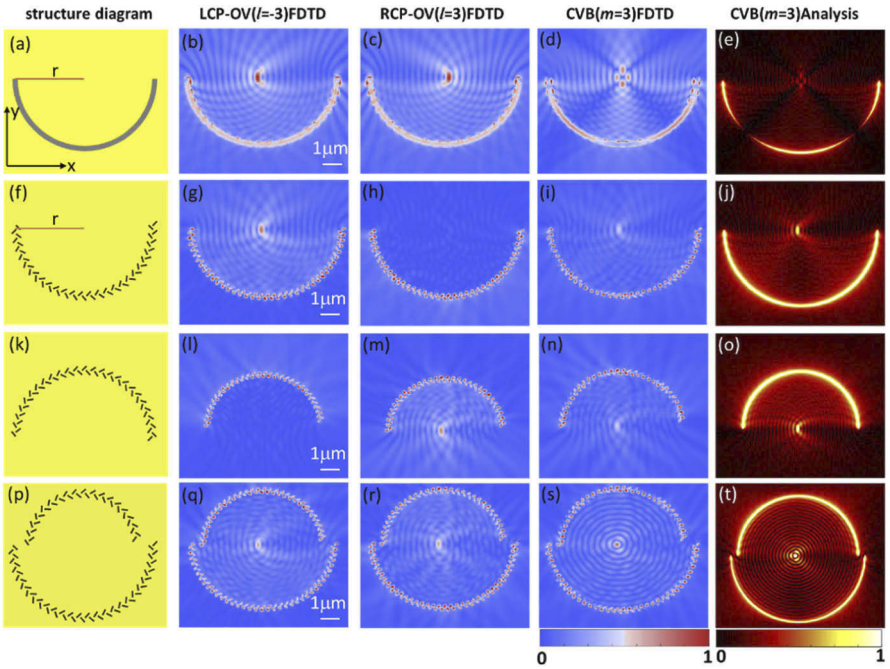

Fig. 2. (a) Schematic diagram of a common plasmonic lens, the FDTD simulated amplitude of E_z component distribution of SPP field when the incident light is (b) an LCP OV with $l = -3$, (c) an RCP OV with $l = 3$ and (d) a CVB with $m = 3$, and (e) the analytical calculation results when the incident light is CVB with $m = 3$. (f)-(j) are similar as (a)-(e) but the structure is a semicircular spin-Hall metalens composed of nano-slit pairs (lower semi-part of the proposed metalens). (k)-(o) are similar as (a)-(e) but the structure is the upper semi-part of the spin-Hall metalens. (p)-(t) are similar as (a)-(e) but the structure is the whole metalens structure.

generate single SPP focus in such case, and the intensity of SPP focus under CVB incidence is obviously stronger than that with only upper or lower half part. In addition, the analytical results (right-most column of Fig. 2) calculated from Eq. (4) well agree with the FDTD simulation results, verifying the correctness of the analytical model.

In order to enhance the intensity of SPP focus for easy detection, more semicircular structures are designed in the spin-Hall metalens. The distance between the two adjacent semicircular structures in upper half and lower half parts is chosen as $\lambda_{spp} \approx 0.6\ \mu m$, and the distance between the two adjacent semicircular structures on the same side is $2\lambda_{spp} \approx 1.2\ \mu m$ to achieve the constructive interference at the focus, as shown in Fig. 3. The incident light is a CVB with $m = 1$ and $\emptyset_0 = 0$ (the well-known radially polarized light). Figures 3(a)-(c) show the E_z component distributions of SPP focal field formed by the metalens with one, two and three rings, respectively, and the profiles of focus along the white horizontal dotted line are compared in Fig. 3(d). It can be observed that as the number of rings (N_r) increases, the intensity of SPP focus increases, due to the constructive interference of SPP generated by each ring. However, it is also found that the side lobes near the central focus of SPP become stronger (Fig. 3(d)) and the growth of focus intensity is slowing down (Fig. 3(e)) with more rings. Thus, the proposed metalens with three rings is finally selected for the following study.

Optics EXPRESS

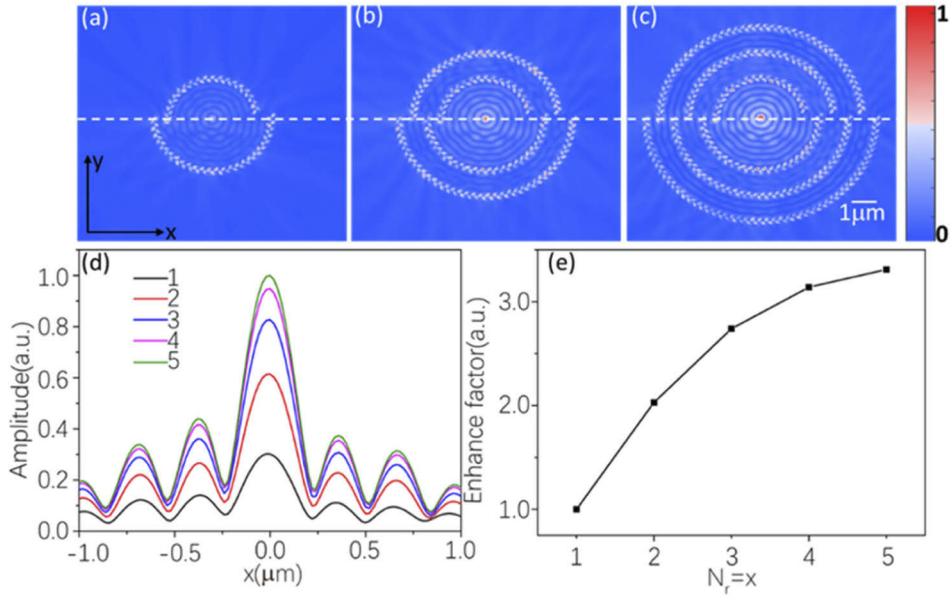

Fig. 3. (a)-(c) The E_z component distributions of SPP focal field formed by the metalens with one, two and three rings, respectively, when the incident light is a CVB with $m = 1$ and $\emptyset_0 = 0$. (d) The E_z amplitude profiles of SPP focus along the white horizontal dashed line when the ring number changes from one to five. (e) The growth of focus intensity as the number of ring changes from one to five.

3.2. *Detection of radial-mode CVBs*

Next, we investigate the detection function of the spin-Hall metalens on the incident CVBs with fixed initial phase angle $\emptyset_0 = 0$ (radial-mode) but different orders m, as shown in the Fig. 4 below. The first column (Figs. 4(a)-(c)) gives three different polarization states of incident CVBs with order $m = -1$, $m = 1$ and $m = 3$, and the second column (Figs. 4(d)-(f)) shows the corresponding E_z component distributions of SPP focal field, respectively. It can be seen in the figure that the focus of SPP is located in the center at $m = 1$, and the focus at $m = -1$ and $m = 3$ moves to the right and left side, respectively. The reason is that in the case of CVB with $m = 1$, both the LCP OV part ($l = -1$ and $\sigma = 1$) and the RCP OV part ($l = 1$ and $\sigma = -1$) have the total angular momentum $j = \sigma + l = 0$ after spin-orbit coupling in SPP excitation, therefore the SPP focal position is located in the center of the metalens. When $m = -1$, for the lower half (upper half) of the metalens, the LCP (RCP) OV is mainly involved, and the total angular momentum after spin-orbit coupling is $j = 2(-2)$, which induces +2 order (-2 order) spiral phase in the lower half (upper half) of the metalens, both making the focus shift to the right side. In the same way, when $m = 3$, the total angular momentum of SPP is -2 (2) for lower (upper) half of the metalens, inducing the -2 order (or+2 order) spiral phase and making the focus shift to the left. To clearly show the shift of the SPP focal point, in Fig. 4(g) we present the profiles of SPP focus along the horizontal x-direction with the incident CVB order ranging from -3 to 3, and the corresponding relationship between the horizontal position of SPP focus and the order of incident CVB is given in Fig. 4(h) with both results of FDTD simulation and analytical calculation. These results demonstrate that the horizontal position of SPP focal point has almost a linear relationship with the CVB order, and the interval between focus points of adjacent CVB orders is about 120 nm. Since the order of CVB corresponds to the SPP focal position one-to-one, the order of CVB can be detected according to the SPP focal position.

Optics EXPRESS

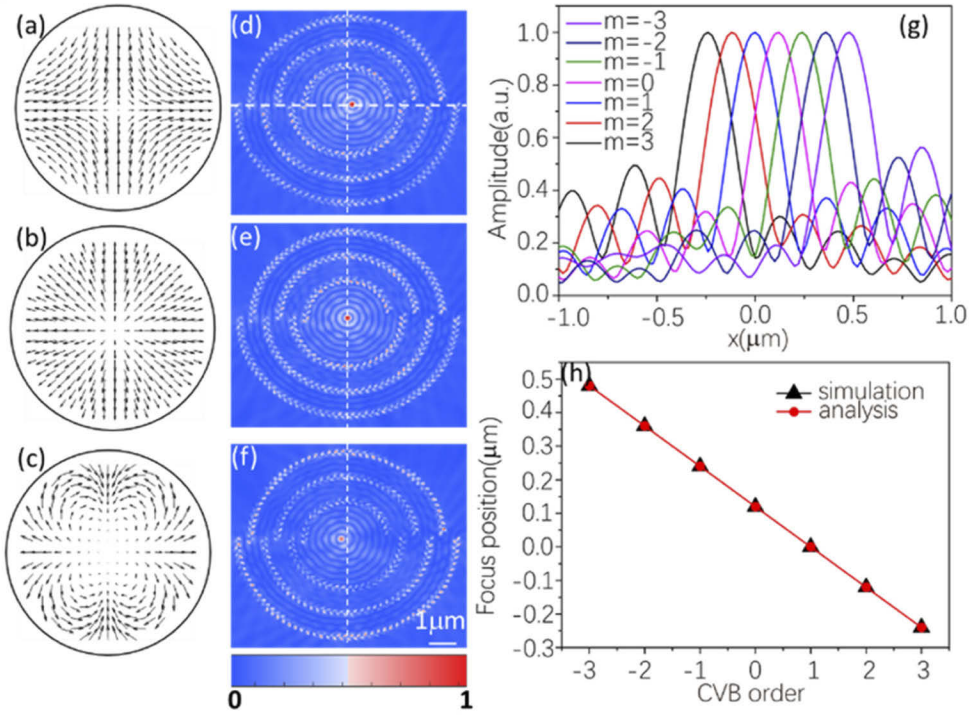

Fig. 4. (a)-(c) The polarization distribution of radially CVB with $m = -1$, $m = 1$ and $m = 3$, respectively, and (d)-(f) are the corresponding Ez component distributions of SPP focal field. (g) The profiles of SPP focus along the horizontal x-direction with the incident CVB order ranging from -3 to 3, and (h) shows the corresponding relationship between the horizontal position of SPP focus and the order m of incident CVB. Both results of FDTD simulation and analytical calculation are shown.

3.3. Detection of azimuthal-mode CVBs

In most previous CVB detection researches, only the CVB order m is detected, while the radial and azimuthal polarization modes of the same order m (corresponding to $\emptyset_0 = 0$ and $\emptyset_0 = \pi/2$ in Eq. (1)) could not be distinguished [42–45]. Here, we demonstrate that the proposed metalens structure can not only detect the the CVB order m, but also distinguish between the radial and azimuthal polarization modes. When the incident light is an azimuthal-mode CVB, taking the azimuthal-mode CVBs with $m = -1$ and $m = 1$ as examples, the corresponding polarization distributions are shown in Fig. 5(a) and Fig. 5(b), respectively. From their E_z component distributions of SPP focal field in Figs. 5(c) and 5(d), it can be found that different to the single SPP focus generated by radial-mode CVBs (Fig. 4), here the SPP focus is split into two symmetry parts with respect to the x-axis. To investigate the splitting effect, the phase distributions of the E_z component are analyzed in Figs. 5(e) and 5(f), which both present a phase difference of π in the center and prove that the destructive interference of SPP excited by the upper and lower parts of the structure results in the splitting of SPP focus. For more CVB orders ranging from -3 to 3, the curves in Fig. 5(g) show their profiles of SPP focus along the vertical line passing through the two split peaks, all presenting the splitting effect and shifting to the $-x$ direction as the order m increasing. The corresponding relationship between the horizontal position of the split SPP focus and the order m of incident azimuthal-mode CVB is given in Fig. 5(h), in which both the results of FDTD simulation and analytical calculation present a nearly linear relationship

Optics EXPRESS

with one-to-one correspondence. Therefore, the proposed metalens structure can also be used to distinguish the radial and azimuthal polarization modes of CVB according to the single or split SPP focus pattern.

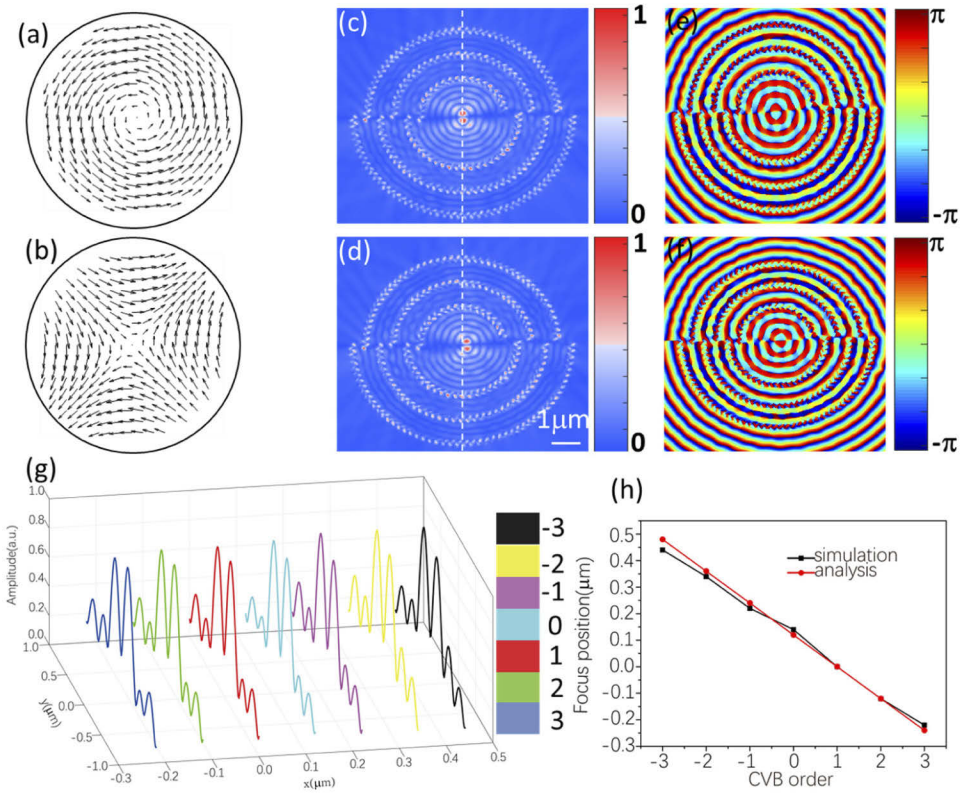

Fig. 5. (a)-(b) The polarization distribution of azimuthal-mdoe CVB with $m = -1$ and $m = 1$, respectively, and (c)-(d) are the corresponding E_z component distributions of SPP focal field. (e)-(f) The corresponding phase distribution of E_z component of SPP focal field. (g) The profiles of SPP focus along the vertical line passing through the two split peaks when the incident light is azimuthal-mode CVB with m changing from -3 to 3. (h) The relationship between the horizontal position of the split SPP focus and the order m of incident azimuthal CVB.

3.4. *Detection of the initial phase angle of CVBs*

Besides the radial and azimuthal polarized modes, we also consider if other vectorial polarization state between the radial and azimuthal modes can be judged according to the splitting effect of the SPP focus, which is equivalent to the detection of initial phase angle of CVBs. When the incident light is CVB with an initial phase angle $\emptyset_0$ between $\emptyset_0 = 0°$ and $\emptyset_0 = 180°$, the distribution of excited SPP field also changes. Taking the CVBs with $\emptyset_0 = 45°$, $\emptyset_0 = 135°$ ($m = 1$) as examples, the polarization distribution of incident CVB is shown in the first column as Figs. 6(a) and 6(b), respectively, and the E_z component distributions of SPP focal field is shown in Figs. 6(c) and 6(d), respectively. It can be found that in these cases, the SPP focus is split into two asymmetry parts with respect to the x-axis. The asymmetry split focus comes from the interference of the SPP excited by the upper and lower parts of the metalens, which is affected by the initial phase of the SPP excited by the upper and lower parts of the metalens (shown in Fig. 6(e) and 6(f)) depending on the $\emptyset_0$ of CVB. The curves shown in Fig. 6(g) show the profiles of asymmetry

Optics EXPRESS

split focus along the vertical line (white dashed line) shown in Fig. 6(c) and Fig. 6(d) when $\emptyset_0$ changing from 0° to 135°, clearly presenting the different splitting shapes of focus at different $\emptyset_0$. To quantify the asymmetry splitting effect, the ratio of peak values of the upper and lower SPP focal points are calculated. Since Fig. 6(g) shows the peak values of the two splitting upper and lower SPP focal points (E_{up} and E_{down} as indicated with black circles in Fig. 6(g)) in respect of the $y = 0$ axis, the ratio value of $(\frac{E_{down}}{E_{up}})$ can be calculated under the CVB incidence with different initial phases. Figure. 6(h) shows the ratio value of $(\frac{E_{down}}{E_{up}})$ between the two asymmetry peaks of SPP focus, in which both FDTD and analytical results verify that the ratio of the two asymmetry peaks changes with the initial phase angle. Thus, this ratio value can be used to judge the initial phase angle $\emptyset_0$ of incident CVB.

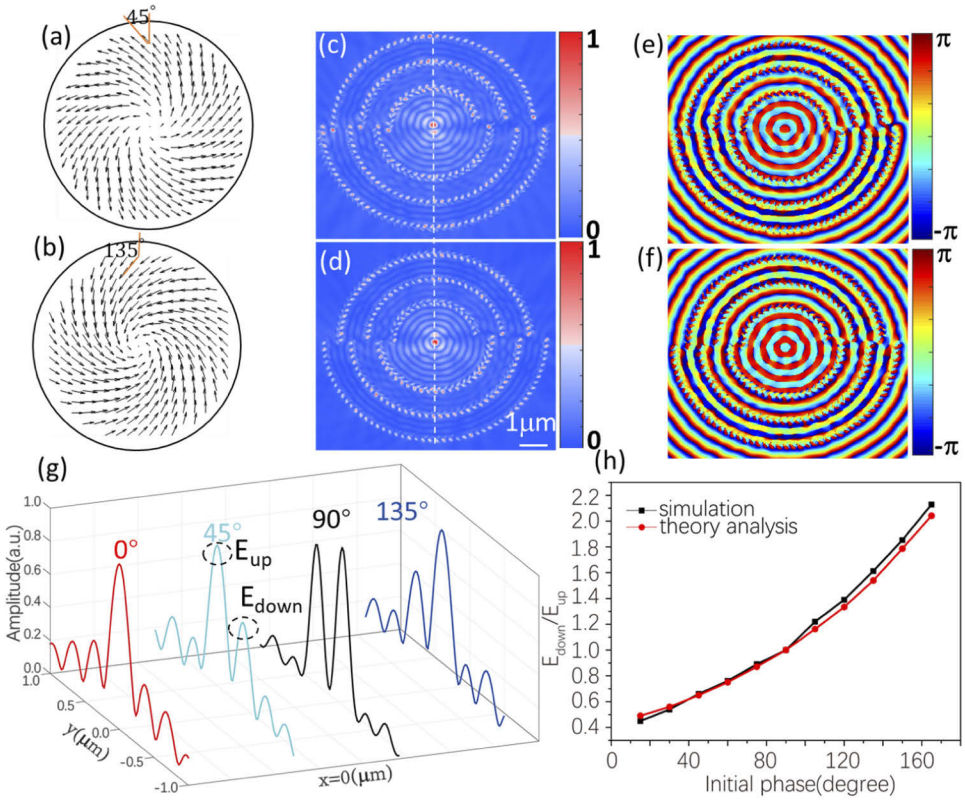

Fig. 6. (a)-(b) The polarization distribution of CVB with $\emptyset_0 = 0°$, $\emptyset_0 = 135°$ ($m = 1$). (c)-(d) The corresponding E_z component distributions of SPP focal field. (e)-(f) The corresponding phase distributions of E_z component of SPP focal field. (g) The profiles of split focus along the vertical lines (as white dashed line in (c) and (d)) when $\emptyset_0$ changing from 0° to 135° with 45° interval. (h) The amplitude ratio between the two asymmetry peaks of SPP focus at different $\emptyset_0$.

4. Conclusion

In this paper, a new method is proposed to realize the on-chip detection of incident CVBs by using a plasmonic spin-Hall metalens composed of orthogonally oriented nano-slits. Both FDTD simulation and theoretical formulas analysis verify that the proposed method can effectively realize microscale detection of polarization order of incident CVB by measuring the shift of

Optics EXPRESS

SPP focus generated by the metalens. Besides the polarization order of CVB, we verify that the designed metalens can also distinguish the orthogonally radial and azimuthal polarization modes under the same CVB order, even other vectorial polarization state between the radial and azimuthal modes can be judged according to the asymmetry splitting effect of the SPP focus, which has not been achieved in most previous works about CVB detection. Although this work is studied with theoretic calculation and simulation, it can be experimentally verified. The proposed metalens can be fabricated by the Electron Beam Lithography (EBL) system like previous works [35,44]. The formed SPP field distribution can be measured by several methods such as a fiber tip-type near-field scanning optical microscope (NSOM) [22,49–51] or Photoelectron Emission Microscopy (PEEM) [52]. This work has potential values in many applications such as CVB multiplexing and processing systems, particle trapping and manipulation, super-resolved imaging, and integrated photonic devices.

Funding. Guangdong Major Project of Basic and Applied Basic Research (2020B0301030009); National Natural Science Foundation of China (62175157, U1701661, 61935013, 61975128, 62105219, 62071306); Leading Talents of Guangdong Province (00201505); Natural Science Foundation of Guangdong Province (2019TQ05X750); Science and Technology Planning Project of Shenzhen Municipality (JCYJ20180507182035270, JCYJ20210324120403011, KQTD20170330110444030, JCYJ20200109113601723, JSGG20210420091805014).

Disclosures. The authors declare no conflicts of interest.

Data availability. Data underlying the results presented in this paper are not publicly available at this time but may be obtained from the authors upon reasonable request.

References

1. M. S. Soskin and M. V. Vasnetsov, "Singular optics," in *Progress in Optics*, E. Wolf, ed. (Elsevier, Amsterdam, 2001).
2. L. Allen, M. W. Beijersbergen, R. J. C. Spreeuw, and J. P. Woerdman, "Orbital Angular-Momentum of Light and the Transformation of Laguerre-Gaussian Laser Modes," Phys. Rev. A **45**(11), 8185–8189 (1992).
3. Q. W. Zhan, "Cylindrical vector beams: from mathematical concepts to applications," Adv. Opt. Photon. **1**(1), 1–57 (2009).
4. W. Wang, T. Yokozeki, R. Ishijima, A. Wada, Y. Miyamoto, M. Takeda, and S. G. Hanson, "Optical vortex metrology for nanometric speckle displacement measurement," Opt. Express **14**(1), 120–127 (2006).
5. C. L. Zhang, C. J. Min, L. P. Du, and X. C. Yuan, "Perfect optical vortex enhanced surface plasmon excitation for plasmonic structured illumination microscopy imaging," Appl. Phys. Lett. **108**(20), 201601–782 (2016).
6. M. F. Andersen, C. Ryu, P. Cladé, V. Natarajan, A. Vaziri, K. Helmerson, and W. D. Phillips, "Quantized rotation of atoms from photons with orbital angular momentum," Phys. Rev. Lett. **97**(17), 170406 (2006).
7. J. Ng, Z. Lin, and C. T. Chan, "Theory of optical trapping by an optical vortex beam," Phys. Rev. Lett. **104**(10), 103601 (2010).
8. F. F. Pang, L. N. Xiang, H. H. Liu, L. Zhang, J. X. Wen, X. L. Zeng, and T. Y. Wang, "Review on Fiber-Optic Vortices and Their Sensing Applications," J. Lightwave Technol. **39**(12), 3740–3750 (2021).
9. C. L. Zhang, R. Wang, C. J. Min, S. W. Zhu, and X. C. Yuan, "Experimental approach to the microscopic phase-sensitive surface plasmon resonance biosensor," Appl. Phys. Lett. **102**(1), 011114 (2013).
10. J. Leach, B. Jack, J. Romero, A. K. Jha, A. M. Yao, and S. Frankearnold, "Quantum correlations in optical angle–orbital angular momentum variables," Science **329**(5992), 662–665 (2010).
11. J. Wang, J. Y. Yang, I. M. Fazal, N. Ahmed, Y. Yan, H. Huang, Y. X. Ren, Y. Yue, S. Dolinar, M. Tur, and A. E. Willner, "Terabit free-space data transmission employing orbital angular momentum multiplexing," Nat. Photonics **6**(7), 488–496 (2012).
12. T. Lei, M. Zhang, Y. Li, P. Jia, G. N. Liu, X. P. Xu, Z. H. Li, C. J. Min, J. Lin, C. Y. Yu, H. B. Niu, and X. C. Yuan, "Massive individual orbital angular momentum channels for multiplexing enabled by Dammann gratings," Light: Sci. Appl. **4**(3), e257 (2015).
13. W. Qiao, T. Lei, Z. T. Wu, S. C. Gao, Z. H. Li, and X. C. Yuan, "Approach to multiplexing fiber communication with cylindrical vector beams," Opt. Lett. **42**(13), 2579–2582 (2017).
14. G. Milione, M. P. Lavery, H. Huang, Y. Ren, G. Xie, T. A. Nguyen, E. Karimi, L. Marrucci, D. A. Nolan, R. R. Alfano, and A. E. Willner, "4 × 20 Gbit/s mode division multiplexing over free space using vector modes and a q-plate mode(de)multiplexer," Opt. Lett. **40**(9), 1980–1983 (2015).
15. R. Chen, K. Agarwal, C. J. Sheppard, and X. Chen, "Imaging using cylindrical vector beams in a high-numerical-aperture microscopy system," Opt. Lett. **38**(16), 3111–3114 (2013).
16. Y. Kozawa and S. Sato, "Optical trapping of micrometer-sized dielectric particles by cylindrical vector beams," Opt. Express **18**(10), 10828–10833 (2010).
17. H. Wang, L. Shi, B. Lukyanchuk, C. Sheppard, and C. T. Chong, "Creation of a needle of longitudinally polarized light in vacuum using binary optics," Nat. Photonics **2**(8), 501–505 (2008).

Optics EXPRESS

18. R. Dorn, S. Quabis, and G. Leuchs, "Sharper focus for a radially polarized light beam," Phys. Rev. Lett. **91**(23), 233901 (2003).
19. M. A. Ahmed, A. Voss, M. M. Vogel, and T. Graf, "Multilayer polarizing grating mirror used for the generation of radial polarization in Yb:YAG thin-disk lasers," Opt. Lett. **32**(22), 3272–3274 (2007).
20. D. Naidoo, F. Roux, A. Dudley, I. Litvin, B. Piccirillo, L. Marrucci, and A. Forbes, "Controlled generation of higher-order Poincaré sphere beams from a laser," Nat. Photonics **10**(5), 327–332 (2016).
21. J. L. Jia, K. P. Zhang, G. W. Hu, M. P. Hu, T. Tong, Q. Q. Mu, H. Gao, F. L. Li, C. W. Qiu, and P. Zhang, "Arbitrary cylindrical vector beam generation enabled by polarization-selective Gouy phase shifter," Photonics Res. **9**(6), 1048–1054 (2021).
22. S. Mei, K. Huang, H. Liu, F. Qin, M. Q. Mehmood, Z. Xu, M. Hong, D. Zhang, J. Teng, A. Danner, and C. W. Qiu, "On-chip discrimination of orbital angular momentum of light with plasmonic nanoslits," Nanoscale **8**(4), 2227–2233 (2016).
23. A. P. Liu, X. Xiong, X. F. Ren, Y. J. Cai, G. H. Rui, Q. W. Zhan, G. C. Guo, and G. P. Guo, "Detecting orbital angular momentum through division-of-amplitude interference with a circular plasmonic lens," Sci. Rep. **3**(1), 2402 (2013).
24. J. Chen, X. Chen, T. Li, and S. Zhu, "On-chip detection of orbital angular momentum beam by plasmonic nanogratings," Laser Photonics Rev. **12**(8), 1700331 (2018).
25. G. Milione, T. A. Nguyen, J. Leach, D. A. Nolan, and R. R. Alfano, "Using the nonseparability of vector beams to encode information for optical communication," Opt. Lett. **40**(21), 4887–4890 (2015).
26. Y. F. Zhao and J. Wang, "High-base vector beam encoding/decoding for visible-light communications," Opt. Lett. **40**(21), 4843–4846 (2015).
27. I. Moreno, J. A. Davis, I. Ruiz, and D. M. Cottrell, "Decomposition of radially and azimuthally polarized beams using a circular polarization and vortex-sensing diffraction grating," Opt. Express **18**(7), 7173–7183 (2010).
28. J. A. Davis, D. M. Cottrell, B. C. Schoonover, J. B. Cushing, J. Albero, and I. Moreno, "Vortex sensing analysis of radially and pseudo-radially polarized beams," Opt. Eng. **52**(5), 050502 (2013).
29. J. C. Fang, Z. W. Xie, T. Lei, C. J. Min, L. P. Du, Z. H. Li, and X. C. Yuan, "Spin-Dependent Optical Geometric Transformation for Cylindrical Vector Beam Multiplexing Communication," ACS Photonics **5**(9), 3478–3484 (2018).
30. D. Wen, J. J. Cadusch, J. Meng, and K. B. Croziera, "Light field on a chip: metasurface-based multicolor holograms," Adv. Photonics **3**(2), 024001 (2021).
31. L. Mao, Y. Li, G. Li, S. Zhang, and T. Cao, "Reversible switching of electromagnetically induced transparency in phase change metasurfaces," Adv. Photonics **2**(05), 056004 (2020).
32. N. F. Yu and F. Capasso, "Flat optics with designer metasurfaces," Nat. Mater. **13**(2), 139–150 (2014).
33. Y. Fu, C. J. Min, J. H. Yu, Z. W. Xie, G. Y. Si, X. Y. Wang, Y. Q. Zhang, T. Lei, J. Lin, D. P. Wang, H. P. Urbachd, and X. C. Yuan, "Measuring phase and polarization singularities of light using spin-multiplexing metasurfaces," Nanoscale **11**(39), 18303–18310 (2019).
34. X. Q. Zhang, Y. H. Xu, W. S. Yue, Z. Tian, J. Q. Gu, Y. F. Li, R. J. Singh, S. Zhang, J. G. Han, and W. L. Zhang, "Anomalous Surface Wave Launching by Handedness Phase Control," Adv. Mater. **27**(44), 7123–7129 (2015).
35. J. Lin, J. P. Balthasar Mueller, Q. Wang, G. H. Yuan, N. Antoniou, X. C. Yuan, and F. Capasso, "Polarization-Controlled Tunable Directional Coupling of Surface Plasmon Polaritons," Science **340**(6130), 331–334 (2013).
36. Z. Wang, S. Q. Li, X. Q. Zhang, X. Feng, Q. W. Wang, J. G. Han, Q. He, W. L. Zhang, S. L. Sun, and L. Zhou, "Excite Spoof Surface Plasmons with Tailored Wavefronts Using High-Efficiency Terahertz Metasurfaces," Adv. Sci. **7**(19), 2000982 (2020).
37. I. Epstein and A. Arie, "Arbitrary Bending Plasmonic Light Waves," Phys. Rev. Lett. **112**(2), 023903 (2014).
38. Y. Q. Zhang, R. R. Zhang, X. Li, L. Ma, C. X. Liu, C. W. He, and C. F. Cheng, "Radially polarized plasmonic vector vortex generated by a metasurface spiral in gold film," Opt. Express **25**(25), 32150–32160 (2017).
39. Z. W. Xie, T. Lei, G. Y. Si, L. P. Du, J. Lin, C. J. Min, and X. C. Yuan, "On-chip spin-controlled orbital angular momentum directional coupling," J. Phys. D: Appl. Phys. **51**(1), 014002 (2018).
40. Y. Meng, Z. T. Liu, Z. W. Xie, R. D. Wang, T. C. Qi, F. T. Hu, H. Kim, Q. R. Xiao, X. Fu, Q. Wu, S. H. Bae, M. L. Gong, and X. C. Yuan, "Versatile on-chip light coupling and (de)multiplexing from arbitrary polarizations to controlled waveguide modes using an integrated dielectric metasurface," Photonics Res. **8**(4), 564–576 (2020).
41. S. Y. Lee, K. Kim, G. Y. Lee, and B. Lee, "Polarization-multiplexed plasmonic phase generation with distributed nanoslits," Opt. Express **23**(12), 15598–15607 (2015).
42. Y. Zhang, P. Li, J. Z. Zhong, S. X. Qi, X. Y. Guo, D. J. Wu, S. Liu, and J. L. Zhao, "Measuring singularities of cylindrically structured light beams using a radial grating," Appl. Phys. Lett. **113**(22), 221108 (2018).
43. J. L. Jia, Z. H. Chang, H. Z. Yang, Q. Liu, F. R. Wang, H. Gao, F. L. and Li, and P. Zhang, "Mode sorter designed for (de)multiplexing vector vortex modes," Appl. Opt. **58**(26), 7094–7099 (2019).
44. F. Feng, G. Y. Si, C. J. Min, X. C. Yuan, and M. Somekh, "On-chip plasmonic spin-Hall nanograting for simultaneously detecting phase and polarization singularities," Light: Sci. Appl. **9**(1), 95 (2020).
45. Z. W. Xie, T. Lei, X. Y. Weng, L. P. Du, S. C. Gao, Y. S. Yuan, S. F. Feng, Y. Zhang, and X. C. Yuan, "A Miniaturized Polymer Grating for Topological Order Detection of Cylindrical Vector Beams," IEEE Photonics Technol. Lett. **28**(24), 2799–2802 (2016).
46. S. S. Kou, G. H. Yuan, Q. Wang, L. P. Du, E. Balaur, D. H. Zhang, D. Y. Tang, B. Abbey, X. C. Yuan, and J. Lin, "On chip photonic Fourier transform with surface plasmon polaritons," Light: Sci. Appl. **5**(2), e16034 (2016).

Optics EXPRESS

47. X. W. Li, L. L. Huang, Q. F. Tan, B. F. Bai, and G. F. Jin, "Integrated plasmonic semi-circular launcher for dielectric-loaded surface plasmon-polariton waveguide," Opt. Express **19**(7), 6541–6548 (2011).
48. G. Li, Y. Sun, and S. Wang, "Spin-Independent Plasmonic Lens," Nanoscale Res. Lett. **14**(1), 156 (2019).
49. H. Kim, J. Park, S. W. Cho, S. Y. Lee, M. Kang, and B. Lee, "Synthesis and dynamic switching of surface plasmon vortices with plasmonic vortex lens," Nano Lett. **10**(2), 529–536 (2010).
50. Z. Shen, Z. J. Hu, G. H. Yuan, C. J. Min, H. Fang, and X. C. Yuan, "Visualizing orbital angular momentum of plasmonic vortices," Opt. Lett. **37**(22), 4627–4629 (2012).
51. A. P. Liu, G. H. Rui, X. F. Ren, Q. W. Zhan, G. C. Guo, and G. P. Guo, "Encoding photonic angular momentum information onto surface plasmon polaritons with plasmonic lens," Opt. Express **20**(22), 24151–24159 (2012).
52. G. Spektor, D. Kilbane, K. Mahro, B. Frank, S. Ristok, L. Gal, P. Kahl, D. Podbiel, S. Mathias, H. Giessen, F. J. M. zu Heringdorf, M. Orenstein, and M. Aeschlimann, "Revealing the subfemtosecond dynamics of orbital angular momentum in nanoplasmonic vortices," Science **355**(6330), 1187–1191 (2017).